RESEARCH ARTICLE | JANUARY 26 2024

Electron and hole bipolar injection in magnesium oxide films

Timofey V. Perevalov ; Damir R. Islamov ; Timur M. Zalyalov ; Andrei A. Gismatulin ; Vladimir A. Golyashov ; Oleg E. Tereshchenko ; Dmitry V. Gorshkov; Vladimir A. Gritsenko

Appl. Phys. Lett. 124, 042903 (2024)
https://doi.org/10.1063/5.0180827

Electron and hole bipolar injection in magnesium oxide films

Cite as: Appl. Phys. Lett. **124**, 042903 (2024); doi: 10.1063/5.0180827
Submitted: 12 October 2023 · Accepted: 1 January 2024 ·
Published Online: 26 January 2024

Timofey V. Perevalov,[1,a)] Damir R. Islamov,[1,2] Timur M. Zalyalov,[1] Andrei A. Gismatulin,[1] Vladimir A. Golyashov,[1] Oleg E. Tereshchenko,[1] Dmitry V. Gorshkov,[3] and Vladimir A. Gritsenko[1,4]

AFFILIATIONS

[1]Rzhanov Institute of Semiconductor Physics, Siberian Branch of the Russian Academy of Sciences, Novosibirsk 630090, Russian Federation
[2]Novosibirsk State University, Novosibirsk 630090, Russian Federation
[3]Katod LTD, Novosibirsk 630047, Russian Federation
[4]Novosibirsk State Technical University, Novosibirsk 630073, Russian Federation

[a)]**Author to whom correspondence should be addressed:** timson@isp.nsc.ru

ABSTRACT

It is assumed that the reliability and functionality of nonvolatile memory elements based on MgO are determined by the charge transport in MgO. In the present study, the type of MgO conductivity is established using experiments on the injection of minority charge-carriers in the *n*(*p*)-Si/MgO/Mg structures. It is shown that electrons and holes contribute to the MgO conductivity, causing bipolar charge transport. Using *ab initio* simulations, it was found that native point defects in MgO can provide both electron and hole conductivity.

Magnesium oxide (MgO) films are currently of great interest for the use as an active layer in the next generation nonvolatile memories. In a spin transfer torque magneto-resistive random access memory (STT-MRAM), a thin MgO film is utilized as a tunnel barrier between two ferromagnetic layers.[1] MgO films also show their resistive switching effect, which is promising for the resistive random access memory (RRAM).[2] The STT-MRAM operating principle is based on the tunneling of spin-polarized electrons through a 2-nm-thick MgO layer.[3] The RRAM operates due to the reversible resistance changing across a dielectric film under the electric field pulse action. It is assumed that both the STT-MRAM and RRAM reliability and functionality are determined by the charge transport in MgO.[4,5] Thus, understanding the charge transport peculiarities in MgO films is an objectively interesting task, the solution of which can be useful for finding ways to improve the STT-MRAM and RRAM characteristics.

The conductivity of inorganic dielectric films can be carried out by electrons and holes.[6,7] A bipolar conduction was observed in a wide range of materials, including Si_3N_4,[8] GeO_2,[9] HfO_2,[10] ZrO_2,[11] and others. Recently, it has been reported that the conductivity of crystal MgO of typical purity is determined by electrons hopping between impurity sites in the crystal.[12] The conductivity in single MgO crystals of nominally the highest purity was proposed to be due to electrons on anion sites corresponding to O^- in the O_2^- structure.[13] The Hall measurements in nanocrystalline MgO films demonstrate that the charge-carriers sign in the longitudinal transport depends on the film thickness, and it changes from a positive to a negative value as soon as the MgO thickness becomes more than 200 nm.[14] Since there is too low charge-carrier concentration in MgO ($\lesssim 3 \times 10^{11}$ cm^{-3}), Hall measurements give significant errors in the charge-carriers sign determination. Moreover, the Hall measurements require a special geometry of test samples, and that is applicable for longitudinal conductivity measurements only. This is not suitable for insulator films in metal–insulator–silicon (MIS) and metal–insulator–metal (MIM) structures. The charge-carriers sign in dielectrics in MIS structures can be determined by the injection of non-equilibrium minority charge-carriers from *n*-Si and *p*-Si substrates generated in the silicon depletion layer.[8]

In this Letter, we report on the charge-carrier sign determination in MgO-based structures Si/MgO/Mg with *n*- and *p*-type silicon substrates. The obtained results will be useful for the development of transport and breakdown in MgO models, especially in CAD computer systems that deal with nonvolatile memory technologies.

MgO films were deposited by the electron-beam method from the MgO granules with a diameter of 1–2 mm and the purity of 99.99%, which were produced by OHARA GmbH, Germany. The residual pressure in the chamber during the MgO spraying is less than 10^{-3} Pa. The MgO deposition rate is 0.1 nm/s. For electrophysical

measurements, 150-nm-thick MgO films were synthesized on the *p*-Si and *n*-Si substrates with the resistance of 10 and 4.5 Ohm × cm, respectively. An upper Mg electrode was deposited on the MgO film through a shadow mask by thermal sputtering with the 0.5 mm^2 area. The lower electrode on the Si substrate was also obtained by the thermal Mg sputtering on the entire non-planar substrate area.

The chemical composition of MgO films synthesized on a *p*-Si substrate was studied using x-ray photoelectron spectroscopy (XPS). The measurements were carried out *ex situ* on an SPECS GmbH Proven x-ARPES system equipped with an ASTRAIOS 190 electron energy analyzer and a 2D-CMOS electron detector. The excitation source was focused monochromatic Al Kα radiation ($h\nu = 1486.7$ eV, 0.5 mm x-ray spot at the 180 W anode power). The XPS spectra were recorded at normal emission and constant pass energy 30 eV with a total energy resolution of <0.6 eV. The spectrometer energy scale was calibrated by setting the measured polycrystalline silver Ag $3d_{5/2}$ level binding energy of 368.22 ± 0.05 eV, with respect to the Fermi energy. Prior to XPS measurements, the samples were degassed by the annealing at ~ 200 °C for 1 h in UHV conditions. The Ar^+ ion etching of the samples surface was carried out using an SPECS IQE 11/35 scanning ion gun with an Ar^+ ions energy of 3 keV, the 45° ion beam incidence angle, and an ion current density of ~ 5 μ A/cm^2.

The current–density vs voltage characteristics (*J*–*V*) and capacitance–voltage (*C*–*V*) ones were measured at room temperature using a Keithley 4200-SCS semiconductor characterization system with 4210-SMU and 4200-CVU units connected to a probe station. The voltage ramp rate used to measure *J*–*V* characteristics was 0.45 V/s.

The *ab initio* simulations of the electronic structure of native point defects in MgO were carried out within the density functional theory (DFT) with the B3LYP exchange-correlation functional in the Quantum ESPRESSO package.[15] The optimized norm-conserving Vanderbilt pseudopotential, the plane wave basis with the 80 Ry cutoff energy, and the 2 × 2 × 2 *k*-point grid were used in the calculations. The defects, namely, O vacancy (O_v), O interstitial (O_{int}), O substituting Mg (O_{subt}), Mg vacancy (Mg_v), Mg interstitial (Mg_{int}), and Mg substituting O (Mg_{subt}), were simulated in the 128-atom supercell. The energy gain, when capturing an additional electron and a hole for a defect, was estimated using the following formula:[16,17]

$$w^{e/h} = \left(E_p^{-1/+1} + E_d^0\right) - \left(E_p^0 + E_d^{-1/+1}\right). \quad (1)$$

Here, E_p^q and E_d^q are perfect and defect supercell total energies, respectively, for the supercell total charge *q*.

First, the chemical composition of the obtained MgO films using XPS was studied. The photoelectron spectra of the Mg2*p* and O1*s* photoemission lines for the initial MgO film surface after the low-temperature annealing (200 °C for 1 h) in ultrahigh vacuum are shown in Figs. 1(a) and 1(b). The Mg2*p* and the most intense O1*s* peaks have binding energies 50.9 and 531.3 eV corresponding to the MgO formation.[18,19] The less intense component of the O1*s* line with the binding energy of 533.2 eV is usually related to the surface contamination or the formation of magnesium hydroxide or carbonate at the MgO surface during the exposure to the atmospheric air.[20] The intensity of this component, as well as of the C1*s* line (not shown) from the surface containing a carbon contamination, is greatly reduced after 5 min of the 3 keV Ar^+ ion etching of the sample surface [red lines in Figs. 1(a) and 1(b)]. The ratio of magnesium and oxygen atomic concentrations

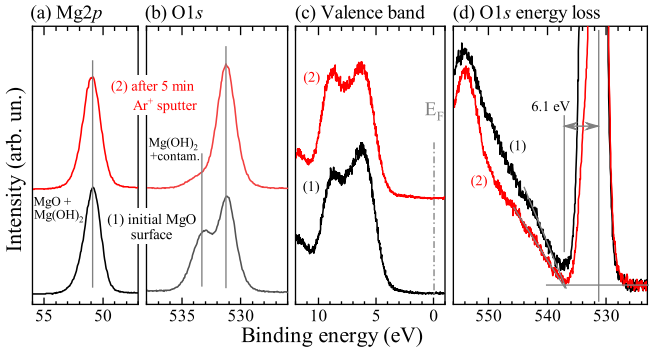

FIG. 1. XPS spectra for the initial 20-nm-thick MgO film surface (1, black lines) and after 5 min of the 3 keV Ar^+ ion etching (2, red lines): (a) Mg2*p* core level, (b) O1*s* core level, and (c) valence band. (d) Level of O1*s* photoelectron energy loss spectra and the MgO bandgap estimation.

estimated from the Mg2*p* and O1*s* line intensities is reduced from [Mg]/[O] = 1±0.15 for the initial MgO surface to [Mg]/[O] = 0.73±0.15 for the ion-treated surface, as expected for the removal of $Mg(OH)_2$ layers. However, ion etching is usually expected to generate oxygen vacancies in oxide dielectrics.[21,22] In our case, no low binding-energy component of the Mg2*p* line, corresponding to the Mg^0 oxidation state, is detectable in the spectra [Fig. 1(a)] after the Ar^+ ion etching. In addition, the valence band spectra [Fig. 1(c)] show no additional defect states formed inside the visible part of the MgO film bandgap similar to that previously reported in Ref. 23 for oxygen-deficient MgO films. One can conclude that the obtained MgO films are near-stoichiometric.

The low-intensity features observed to the higher binding energy of the main O1*s* peak [Fig. 1(d)] reflect the photoelectron energy loss spectrum due to the excitation of electron transitions from the valence band to the conduction band. It allows the bandgap energy value E_g estimation. E_g is determined by the linear interpolation of the edge of the excitation spectrum from inter-band transitions to the background level. The estimation of the E_g value yields about 6.1 eV. This result is in a good agreement with the values previously determined for MgO from scanning tunneling microscopy and from the internal photoemission of electrons and holes.[24,25]

Knowing this value, as well as the E_v position relative to the vacuum level for Si (5.2 eV),[26] the MgO electron affinity (1.0 eV),[27,28] and the electron work function for Mg (3.6 eV),[29] one can construct an energy diagram for the Si/MgO/Mg structure, as shown in Fig. 2(a). This is a simplified diagram in the flatband mode that does not consider the localization of electrons and holes in the dielectric, as well as the SiO_x interlayer on the Si substrate. One can see that the barrier for holes $\Phi_h = 2.0$ eV in the Si/MgO interface is lower than that for electrons $\Phi_e = 3.0$ eV. It is interesting to note that, previously, a reverse result was obtained ($\Phi_e = 2.3$ eV and $\Phi_h = 2.7$ eV) from the internal photoemission experiments,[25] but these values predict an overestimated MgO electron affinity.

When a positive potential for *n*-Si/MgO/Mg is applied to Mg, the electron system is in the accumulation mode. The *J*–*V* characteristics in the accumulation mode demonstrate an exponential dependence on the applied voltage and the absence of the illumination influence on the current density value [Fig. 2(d)]. The currents through the *n*-Si/

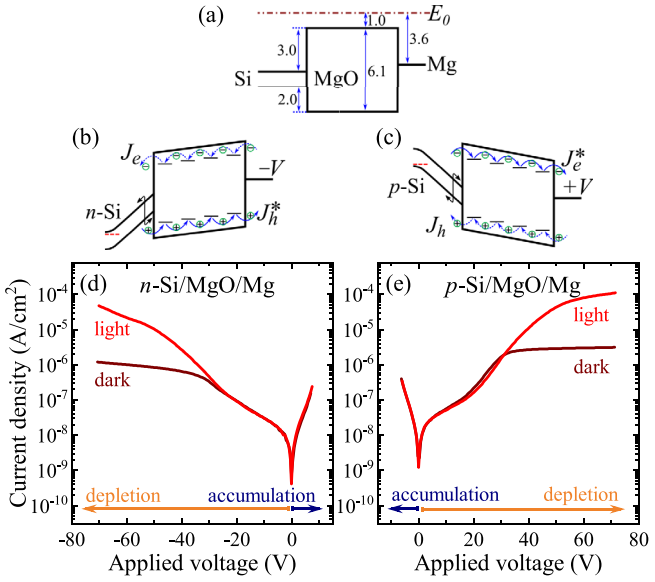

FIG. 2. Energy diagram Si/MgO/Mg structures: (a) in the flatband mode, (b) *n*-Si/MgO/Mg, and (c) *p*-Si/MgO/Mg structures in the depletion mode. J_e^*/J_h^* and J_e/J_h are flows of injected minority electrons/holes from Si into MgO and from Mg into MgO, respectively. *J*–*V* characteristics of Si/MgO/Mg structures in the dark and under lighting in accumulation and depletion modes: (d) *n*-Si/MgO/Mg and (e) *p*-Si/MgO/Mg.

MgO/Mg structure are determined by the injection of majority charge-carriers from Si substrate to MgO (namely, electrons) and/or by injected holes from the metal electrode to MgO. When a negative potential for *n*-Si/MgO/Mg is applied to the metal contact, the electron system falls in the non-equilibrium depletion mode. In the depletion mode, the currents exhibit their saturation at a relatively high voltage $|V| > 30$ V. In this mode, the majority charge-carriers in the silicon substrates are pulled out by a strong electric field from the Si/MgO interface to the Si bulk. The currents in the dark are limited by thermal generated minority carriers (holes) or by the injected electrons from the metal electrode [J_e in Fig. 2(b)]. When the structure is illuminated, no extra charge-carriers are generated in a metal electrode, but, in the silicon depletion region, light absorption leads to the non-equilibrium electron–hole pair generation [curve arrow in Fig. 2(b)]. Here, the majority charge-carriers in the silicon substrates are pulled out by a strong electric field from the Si/MgO interface to the Si bulk, while the extra minority charge-carriers (holes) are electrostatically attracted to the Si/MgO interface. As far as the current saturation level in the *J*–*V* plate for the non-equilibrium depletion mode arises, one can conclude that the holes are able to flow through the dielectric layer.

The same phenomena take place for *p*-Si/MgO/Mg structures. In the accumulation mode, when a negative potential is applied to the Mg contact, the *J*–*V* characteristics do not depend on illumination and exhibit their exponential dependence, as shown in Fig. 2(e). In the depletion mode (when a positive potential is applied to the metal electrode), the current saturation level increases under illumination due to the additional flow of non-equilibrium minority electrons generated in the substrate depletion region [curve arrow and J_e^* in Fig. 2(c)]. Thus, the MgO film conductivity can be carried out by both electrons and holes injected from silicon. In other words, the MgO film conductivity is bipolar.

One can see that the current saturation levels are close for *n*- and *p*-type substrates [Figs. 2(d) and 2(e)], while the recently observed data for other dielectric materials exhibit quite different levels.[8–11] Indeed, in the non-equilibrium depletion mode of silicon in MIS structures, the current saturation might be denoted as $J^* = qG^*\tau^*/\tau_{tr}$, where q is the elementary charge, G^* is the non-equilibrium electron–hole pair generation rate, τ^* is the mean lifetime of minority charge-carrier, and τ_{tr} is the mean time of the appropriate charge-carrier transfer through the dielectric layer. Thus, the obtained data include a complex combination of three parameters if one tries to analyze the current saturation level quantitatively. Moreover, the G^* value might fluctuate from contact-to-contact even on a single substrate because it depends on the geometry factors of the metal contact, including the local thickness due to high light absorption in metals. That is why the obtained results are qualitative.

Independent confirmations of the charge-carrier of both signs injection from Si and Mg into MgO can be obtained from the shift of the capacitance–voltage (*C*–*V*) characteristic (Fig. 3). To do this, initial (pristine) *C*–*V* characteristics were measured with a voltage sweep −2 to 0 V at which there is no charge trapping in the MgO layer due to applied voltage. When a voltage of such small amplitude is applied from depletion to saturation and *vice versa*, the *C*–*V* characteristic has no hysteresis, as shown by the black curve in Figures 3(a) and 3(b). The voltage sweep with a higher amplitude might provide a charge

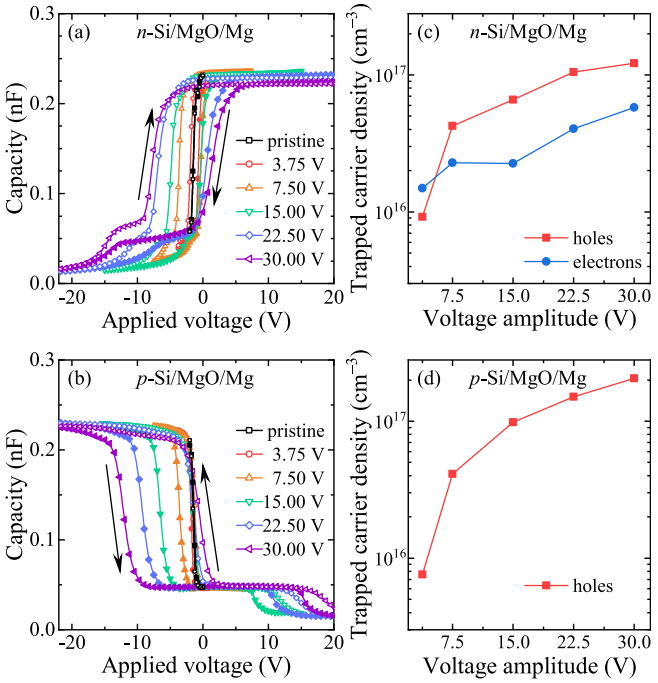

FIG. 3. *C*–*V* characteristics of Si/MgO/Mg structures: (a) *n*-Si/MgO/Mg and (b) *p*-Si/MgO/Mg. Black (pristine) curves are measured with the voltage sweep from −2 to 0 V. Filled symbols indicate the voltage sweep from accumulation to depletion modes; empty ones—the voltage sweep from depletion to accumulation modes, as shown by black arrows. Trapped carrier density as a function of voltage amplitude: (c) *n*-Si/MgO/Mg and (d) *p*-Si/MgO/Mg.

injection into the dielectric from electrodes, and that is indicated by the hysteresis in the C–V plate. The comparison of left and right C–V branches against the initial curve allows one to extract the trapped charge in the dielectric layer of the MIS structure. For the n-Si/MgO/Mg structure, when a positive potential is applied to Mg, the C–V characteristic shifts to the right, relative to the initial curve, thus indicating the negative charge accumulation. This is the charge from electrons injected from n-Si (accumulation mode) and localized on the traps in MgO [Fig. 3(a)]. The shift ΔV allows one to extract the trapped electron density n_t. In the case of uniform charge distribution in the MgO layer, it might be found as follows:

$$n_t = C_{max}\Delta V/q, \tag{2}$$

where C_{max} is the maximum capacitance of the MIS structure. After a negative potential is applied, the C–V characteristic shifts to the left, indicating the accumulation of a positive charge of holes. The trapped hole density p_t can be denoted in the same way as Eq. (2),

$$p_t = C_{max}(-\Delta V)/q. \tag{3}$$

The dependences of n_t and p_t as functions of the voltage sweep amplitude for n-Si/MgO/Mg structure are shown in Fig. 3(c). For the p-Si/MgO/Mg structure, the negative potential on Mg shifts the C-V curves to the left [Fig. 3(b)]. This is explained by the accumulation of positive charge from holes injected from p-Si and localized on the hole traps in MgO [Figs. 3(b) and 3(d)]. The application of the positive voltage to the Mg contact slightly shifts the C–V curves, and that corresponds to much lower values in comparison with p_t (that is why the n_t values for the case of p-Si are not shown). As the result, both electrons from n-Si and holes from p-Si are injected into MgO when the corresponding potential is applied. This confirms that the MgO conductivity is bipolar.

According to the DFT simulation, almost for all types of native point defects in c-MgO (except for Mg_v), the values of w^e and w^h are positive (Table I). Hence, the capture of both an electron and a hole on these defects is energetically favorable. The energy gain, when capturing an electron/hole, is, essentially, the energy of a thermal ionization trap. Assuming the hopping conductivity by defects, it can be expected that defects with a relatively small w^e and w^h value participate in the charge transport. However, it is unknown what defect types are present and dominate in real MgO films. Nevertheless, one can say that O_v, Mg_{int}, and Mg_{subt} are involved in the electron transport, and O_{int} and O_{subt} are in the hole transport. At the same time, O_v and O_{int} are amphoteric traps, i.e., capable of capturing both an electron and a hole. Probably, O_v and O_{int} are the key defects responsible for the bipolar MgO conductivity. It is worth noting that the trap energy value error by the method used in the studies is about 0.3 eV, judging by the experience of various dielectric simulations. Taking into account that cubic MgO with $E_g = 7.2$ eV is used in the simulation, the error in the overestimation direction may be greater. Nevertheless, even taking into account possible errors of the method, this does not change the main conclusion that, in MgO, intrinsic defects can participate in both the electron and hole charge conductivity. The transport of charge-carriers (electrons and holes) by hops between traps caused by defects present in MgO films is schematically shown by blue arrows in Figures 2(b) and 2(c).

TABLE I. Calculated values (in eV) of w^e and w^h for native point defects in c-MgO: the O/Mg vacancy, O/Mg interstitial, and O/Mg substitutional.

	O_v	O_{int}	O_{subt}	Mg_v	Mg_{int}	Mg_{subt}
w^e	0.6	2.6	6.8	7.3	1.1	1.8
w^h	3.6	0.4	1.0	<0	6.9	6.1

To sum it up, the energy diagram of the Si/MgO/Mg structure was constructed. The saturation current in the depletion mode in the n-Si/MgO/Mg and p-Si/MgO/Mg structures and an increase in the current level under illumination indicate the electron and hole injection, respectively, from the silicon substrate into MgO. The confirmations of the minority carrier of both sign injection from Si into MgO were obtained from the shift of the capacitance–voltage characteristic due to the accumulation of a positive and negative charge under the sufficient applied potential. Using the *ab initio* simulations, it was found that various types of native point defects (vacancies, interstitial atoms, and substitution defects) in c-MgO can provide both electron and hole conductivity. It is suggested that O_v and O_{int} are the key defects that are traps for both electrons and holes involved in the charge transport. Thus, the MgO conductivity in the Si/MgO/Mg structure is bipolar. Electrons are injected into MgO from the electrode with a negative potential, and, accordingly, holes are injected from the electrode with a positive potential.

This work was supported by the Ministry of Science and Higher Education of the Russian Federation: Grant No. 075-15-2020-797 (13.1902.21.0024). The electrophoretic measurements were made on the equipment of CKP "VTAN" at the ATRC Department of NSU. The *ab initio* simulations were carried out at the NSU Supercomputer Center.

AUTHOR DECLARATIONS

Conflict of Interest

The authors have no conflicts to disclose.

Author Contributions

Timofey Viktorovich Perevalov: Conceptualization (equal); Formal analysis (equal); Investigation (equal); Writing – original draft (equal); Writing – review & editing (equal). **Damir R. Islamov:** Formal analysis (equal); Writing – original draft (equal); Writing – review & editing (equal). **Timur Maratovich Zalyalov:** Formal analysis (equal); Investigation (equal); Methodology (equal). **Andrei A. Gismatulin:** Formal analysis (equal); Investigation (equal). **Vladimir A. Golyashov:** Formal analysis (equal); Methodology (equal); Visualization (equal); Writing – original draft (equal). **Oleg E. Tereshchenko:** Formal analysis (equal); Methodology (equal). **Dmitry Valerievich Gorshkov:** Resources (equal). **Vladimir A. Gritsenko:** Conceptualization (equal); Funding acquisition (equal); Project administration (equal).

DATA AVAILABILITY

The data that support the findings of this study are available from the corresponding author upon reasonable request.

REFERENCES

[1]F. Schleicher, U. Halisdemir, D. Lacour, M. Gallart, S. Boukari, G. Schmerber, V. Davesne, P. Panissod, D. Halley, H. Majjad, Y. Henry, B. Leconte, A.

Boulard, D. Spor, N. Beyer, C. Kieber, E. Sternitzky, O. Cregut, M. Ziegler, F. Montaigne, E. Beaurepaire, P. Gilliot, M. Hehn, and M. Bowen, Nat. Commun. **5**, 4547 (2014).
[2]J. Guo, S. Ren, L. Wu, X. Kang, W. Chen, and X. Zhao, Appl. Surf. Sci. **434**, 1074 (2018).
[3]S. S. P. Parkin, C. Kaiser, A. Panchula, P. M. Rice, B. Hughes, M. Samant, and S.-H. Yang, Nat. Mater. **3**, 862 (2004).
[4]H. L. Meyerheim, R. Popescu, J. Kirschner, N. Jedrecy, M. Sauvage-Simkin, B. Heinrich, and R. Pinchaux, Phys. Rev. Lett. **87**, 076102 (2001).
[5]W. H. Butler, X.-G. Zhang, T. C. Schulthess, and J. M. MacLaren, Phys. Rev. B **63**, 054416 (2001).
[6]F. H. Hielscher and H. M. Preier, Solid-State Electron. **12**, 527 (1969).
[7]K. A. Nasyrov and V. A. Gritsenko, Phys.-Usp. **56**, 999 (2013).
[8]K. A. Nasyrov, V. A. Gritsenko, Y. N. Novikov, E.-H. Lee, S. Y. Yoon, and C. W. Kim, J. Appl. Phys. **96**, 4293 (2004).
[9]D. R. Islamov, V. A. Gritsenko, C. H. Cheng, and A. Chin, Appl. Phys. Lett. **103**, 232904 (2013).
[10]D. R. Islamov, V. A. Gritsenko, C. H. Cheng, and A. Chin, Appl. Phys. Lett. **99**, 072109 (2011).
[11]D. R. Islamov, V. A. Gritsenko, T. V. Perevalov, V. S. Aliev, V. A. Nadolinny, and A. Chin, Materialia **15**, 100980 (2021).
[12]S. P. Mitoff, J. Chem. Phys. **31**, 1261 (1959).
[13]H. Kathrein and F. Freund, J. Phys. Chem. Solids **44**, 177 (1983).
[14]M. H. Al-Timimi, W. H. Albanda, and M. Z. Abdullah, East Eur. J. Phys. **2**, 173 (2023).
[15]P. Giannozzi, O. Andreussi, T. Brumme, O. Bunau, M. B. Nardelli, M. Calandra, R. Car, C. Cavazzoni, D. Ceresoli, M. Cococcioni, N. Colonna, I. Carnimeo, A. D. Corso, S. de Gironcoli, P. Delugas, R. A. DiStasio, A. Ferretti, A. Floris, G. Fratesi, G. Fugallo, R. Gebauer, U. Gerstmann, F. Giustino, T. Gorni, J. Jia, M. Kawamura, H.-Y. Ko, A. Kokalj, E. Küçükbenli, M. Lazzeri, M. Marsili, N. Marzari, F. Mauri, N. L. Nguyen, H.-V. Nguyen, A. O-d l Roza, L. Paulatto, S. Poncé, D. Rocca, R. Sabatini, B. Santra, M. Schlipf, A. P. Seitsonen, A. Smogunov, I. Timrov, T. Thonhauser, P. Umari, N. Vast, X. Wu, and S. Baroni, J. Phys.: Condens. Matter **29**, 465901 (2017).
[16]A. S. Foster, F. Lopez Gejo, A. L. Shluger, and R. M. Nieminen, Phys. Rev. B **65**, 174117 (2002).
[17]T. V. Perevalov and D. R. Islamov, Microelectron. Eng. **216**, 111038 (2019).
[18]J. S. Corneille, J.-W. He, and D. W. Goodman, Surf. Sci. **306**(3), 269 (1994).
[19]R. Lewandków, P. Mazur, A. Trembułowicz, A. Sabik, R. Wasielewski, and M. Grodzicki, Materials **14**, 4189 (2021).
[20]V. Rheinheimer, C. Unluer, J. Liu, S. Ruan, J. Pan, and P. Monteiro, Materials **10**, 75 (2017).
[21]T. V. Perevalov, A. A. Gismatulin, D. S. Seregin, Y. Wang, H. Xu, V. N. Kruchinin, E. V. Spesivcev, V. A. Gritsenko, K. A. Nasyrov, I. P. Prosvirin, J. Zhang, K. A. Vorotilov, and M. R. Baklanov, J. Appl. Phys. **127**, 195105 (2020).
[22]T. V. Perevalov, D. R. Islamov, V. A. Gritsenko, and I. P. Prosvirin, Nanotechnology **29**, 194001 (2018).
[23]Y. Wan, C. Samundsett, J. Bullock, M. Hettick, T. Allen, D. Yan, J. Peng, Y. Wu, J. Cui, A. Javey, and A. Cuevas, Adv. Energy Mater. **7**, 1601863 (2017).
[24]P. G. Mather, J. C. Read, and R. A. Buhrman, Phys. Rev. B **73**, 205412 (2006).
[25]V. V. Afanas'ev, A. Stesmans, K. Cherkaoui, and P. K. Hurley, Appl. Phys. Lett. **96**, 052103 (2010).
[26]D. T. Pierce and W. E. Spicer, Phys. Rev. B **5**, 3017 (1972).
[27]J. R. Stevenson and E. B. Hensley, J. Appl. Phys. **32**, 166 (1961).
[28]M. O. Aboelfotoh and J. A. Lorenzen, J. Appl. Phys. **48**, 4754 (1977).
[29]N. D. Lang and W. Kohn, Phys. Rev. B **3**, 1215 (1971).